Acoustical Physics, Vol. 50, No. 5, 2004, pp. 512–517. Translated from Akusticheskiĭ Zhurnal, Vol. 50, No. 5, 2004, pp. 603–608.

Electroacoustic Lamb Waves in Piezoelectric Crystal Plates

M. Yu. Dvoesherstov, V. I. Cherednik, and A. P. Chirimanov

Lobachevskii State University, Nizhni Novgorod, pr. Gagarina 23, Nizhni Novgorod, 603950 Russia

e-mail: dvoesh@rf.unn.ru

Received April 3, 2003

Abstract—The main characteristics of various types of plate electroacoustic waves propagating in piezoelectric single-crystal plates of various thickness are numerically studied. A number of piezoelectric plates and orientations in them with record high values of the electromechanical coupling coefficient for transverse plate waves are proposed. © *2004 MAIK "Nauka/Interperiodica".*

As is well known [1–5], a set of plate waves of two classes, Lamb waves and transverse waves, can propagate in a piezoelectric crystal plate. Plate waves propagating in piezoelectric crystal plates provide the basis for developing a variety of acoustoelectronic pressure and temperature sensors, gas and liquid analyzers, and so on [6–8].

The objective of the present study is the numerical analysis of the main parameters of various types of plate waves propagating in plates (whose thickness H is comparable with the wavelength λ) made of piezoelectric single crystals of any crystallographic symmetry class. For various piezoelectric crystal plates, a theoretical search for orientations corresponding to the optimal parameters of plate waves (a high electromechanical coupling coefficient K^2 and a minimal temperature coefficient of delay) is performed.

Figure 1 shows the coordinate system for the problem under investigation. Let the X_1 axis be the direction of wave propagation and the X_3 axis be perpendicular to the plane of a plate of thickness H. For convenience, we place the plane $X_3 = 0$ in the middle of the plate.

As is known [9], acoustic waves propagating in isotropic plates are subdivided into two classes: Lamb waves with vertical-longitudinal polarization and plate waves with transverse polarization (SH waves [1, 5]). In piezoelectric crystal plates, depending on the crystal symmetry class and the specific direction in the crystal, plate waves may have various structures, but they are always accompanied by a quasistatic electric field. The analysis of the properties of plate waves propagating in a piezoelectric plate of any crystallographic symmetry class and any orientation can be performed only by a numerical method. In the analysis, the standard Farnell–Jones technique [10] can be used. The general solution for the mechanical displacements u_i and the electric potential φ can be represented as a sum of eight partial waves:

$$u_i = \sum_{n=1}^{8} A_n \alpha_i^{(n)} \exp(i\kappa\beta^{(n)} X_3) \exp\{i\kappa[X_1 - Vt]\},$$
$$\varphi = \sum_{n=1}^{8} A_n \alpha_4^{(n)} \exp(i\kappa\beta^{(n)} X_3) \exp\{i\kappa[X_1 - Vt]\}. \quad (1)$$

Here, $\alpha_i^{(n)}$ (i = 1, 2, 3) and A_n are the amplitude coefficients, $\beta^{(n)}$ are the attenuation coefficients along the X_3 axis, κ is the wave number, V is the velocity of wave propagation, and t is time. Substituting general solution (1) into the coupled equations of the theory of elasticity for a piezoelectric medium [10], we obtain the Christoffel matrix equation (Eq. (2) below), from which all eight attenuation coefficients $\beta^{(n)}$ (n = 1–8) and the amplitude coefficients $\alpha_i^{(n)}$ can be found:

$$\begin{pmatrix} G_{11} & G_{12} & G_{13} & G_{14} \\ G_{21} & G_{22} & G_{23} & G_{24} \\ G_{31} & G_{32} & G_{33} & G_{34} \\ G_{41} & G_{42} & G_{43} & G_{44} \end{pmatrix} * \begin{pmatrix} \alpha_1 \\ \alpha_2 \\ \alpha_3 \\ \alpha_4 \end{pmatrix} = 0. \quad (2)$$

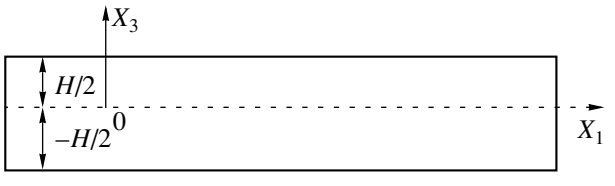

Fig. 1. The coordinate system.

1063-7710/04/5005-0512$26.00 © 2004 MAIK "Nauka/Interperiodica"

Here,

$$\begin{aligned}
G_{11} &= C_{55}^*\beta^2 + 2^*C_{15}^*\beta + C_{11} - \rho^*V^2,\\
G_{12} &= G_{21} = C_{45}^*\beta^2 + (C_{14} + C_{56})^*\beta + C_{16},\\
G_{13} &= G_{31} = C_{35}^*\beta^2 + (C_{13} + C_{55})^*\beta + C_{15},\\
G_{14} &= G_{41} = e_{35}^*\beta^2 + (e_{15} + e_{31})^*\beta + e_{11},\\
G_{22} &= C_{44}^*\beta^2 + 2^*C_{46}^*\beta + C_{66} - \rho^*V^2\\
G_{23} &= G_{32} = C_{34}^*\beta^2 + (C_{36} + C_{45})^*\beta + C_{56},\\
G_{24} &= G_{42} = e_{34}^*\beta^2 + (e_{14} + e_{36})^*\beta + e_{16},\\
G_{33} &= C_{33}^*\beta^2 + 2^*C_{35}^*\beta + C_{55} - \rho^*V^2,\\
G_{34} &= G_{43} = e_{33}^*\beta^2 + (e_{13} + e_{35})^*\beta + e_{15},\\
G_{44} &= -(\varepsilon_{33}^*\beta^2 + 2^*\varepsilon_{13}^*\beta + \varepsilon_{11}),
\end{aligned} \tag{3}$$

where C_{ij}, e_{ij}, and ε_{ij} are the tensors of elastic, piezoelectric, and dielectric constants of the material represented in the contracted matrix form [10] and ρ is the density of the material.

Note that, depending on the crystal symmetry and direction of wave propagation [11], Eq. (2) may be confluent and simultaneously have two independent solutions, because zero terms may appear in it. If the following conditions are satisfied for the elastic and piezoelectric constants of the piezoelectric crystal in the accepted coordinate system,

$$\begin{aligned}
C_{14} = C_{16} = C_{34} = C_{36} = C_{45} = C_{56} = 0;\\
e_{14} = e_{16} = e_{34} = e_{36} = 0,
\end{aligned} \tag{4}$$

one of the independent solutions of Eq. (2) corresponds to piezoactive Lamb modes of the vertical-longitudinal polarization with two components of mechanical displacement and an electric potential (u_1, u_3, and φ), and the other independent solution corresponds to a nonpiezoactive, purely transverse wave with one transverse component of mechanical displacement u_2. If the condition

$$\begin{aligned}
C_{14} = C_{16} = C_{34} = C_{36} = C_{45} = C_{56} = 0;\\
e_{11} = e_{13} = e_{15} = e_{31} = e_{33} = e_{35} = 0
\end{aligned} \tag{5}$$

is satisfied, one of the independent solutions corresponds to a piezoactive plate wave of the transverse polarization with one transverse displacement component and an electric potential (u_2, φ) and the other independent solution corresponds to nonpiezoactive Lamb modes of vertical-longitudinal polarization with two components of mechanical displacement (u_1, u_3).

Thus, if the symmetry conditions (4) and (5) are satisfied, Eq. (2) will always have two independent solutions for Lamb modes of any order, because the symmetry conditions (4) and (5) and their effect on Eq. (2) do not depend on the boundary conditions.

For the most general case of crystal symmetry, Eq. (2) has a unique solution and the modes propagating in the piezoelectric plate have all three components of mechanical displacement and an electric potential (u_1, u_2, u_3, and φ).

To determine the unknown amplitude coefficients A_n, it is necessary to use eight boundary conditions at the upper ($X_3 = H/2$) and lower ($X_3 = -H/2$) boundaries of the piezoelectric plate. These conditions are the zero value of the normal components of the stress tensor at the upper and lower boundaries of the plate

$$T_{31} = 0, \quad T_{32} = 0, \quad T_{33} = 0 \text{ for } X_3 = \pm H/2; \tag{6}$$

the continuity of the normal component of the electric induction at the boundary between the piezoelectric plate and the vacuum (for an open surface)

$$D_3 = D_3^{\text{vac}} \text{ for } X_3 = H/2 \text{ and (or) } X_3 = -H/2 \tag{7a}$$

or the zero value of the electric potential at the boundary when the surface is short-circuited (metallized)

$$\varphi = 0 \text{ for } X_3 = H/2 \text{ and (or) } X_3 = -H/2. \tag{7b}$$

Then, substituting general solutions (1) into boundary conditions (6) and (7), we obtain a set of homogeneous complex boundary equations, the solution of which yields the unknown amplitude coefficients A_n and phase velocities V_k of all modes propagating in the piezoelectric plate.

One of the difficulties arising in the numerical search for the plate wave solutions consists in the fact that, in a piezoelectric plate of a certain thickness H, there is a family of plate modes and each mode has its own phase velocity V_k. Therefore, in the search for every individual mode (search for the zero of the function of boundary equations), it is necessary to choose a sufficiently narrow interval of the velocity search ΔV that would contain only two values of velocity for the same mode: for an open and a short-circuited surface (to calculate the electromechanical coupling coefficient K^2). For a reliable determination of such an interval, we visualized the plot of the function of boundary conditions in the program window.

After finding the phase velocity V_k of some mode, it is possible to determine the electromechanical coupling coefficient (K^2). Usually, the electromechanical coupling coefficient for a surface acoustic wave (SAW) is calculated from the expression [10]

$$K^2 = 2(V_0 - V_S)/V_0, \tag{8}$$

where V_0 and V_S are the phase velocities of the wave at the open and metallized surfaces of the crystal, respectively. For a semi-infinite crystal, this quantity is single-valued for the given orientation. This relation can also be used for calculating the value of K^2 for plate waves.

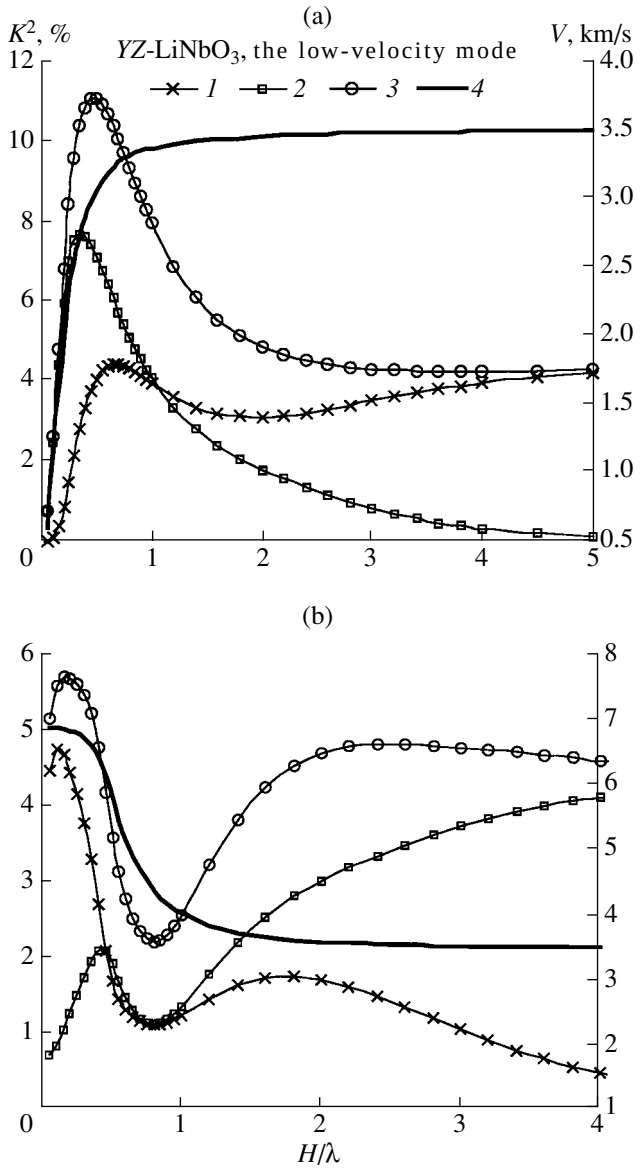

Fig. 2. (*1–3*) Electromechanical coupling coefficient K^2 and (*4*) the velocity of SAW propagation V versus the normalized plate thickness H/λ for the (a) low-velocity and (b) high-velocity zero-order mode. The lower surface is (*1*) open or (*2*) short-circuited; (*3*) both surfaces are either open or short-circuited.

In this case, the electromechanical coupling coefficient K^2 for different modes has a spatial dispersion (it depends on the relative thickness of the piezoelectric plate H/λ).

Note that the phase velocity of plate waves in a piezoelectric plate also depends on the electrical boundary conditions at the lower boundary of the plate (an open or short-circuited surface). Hence, in calculating the electromechanical coupling coefficient K^2 from the relative difference in the velocities along the open and short-circuited surfaces, one should take into account the electrical boundary conditions at the lower surface, which may be either open or short-circuited. If the lower surface is electrically short-circuited, the mode velocities will differ from the velocities for an open lower surface. The electromechanical coupling coefficient K^2 calculated from Eq. (8) will also differ in this case. And, finally, instead of V_0 in Eq. (8), one can substitute the velocity corresponding to both surfaces being open, and instead of V_S, the velocity corresponding to both surfaces being short-circuited. Thus, it is possible to obtain three values of the electromechanical coupling coefficient K_i^2 (i = 1–3), which correspond to three different ways of short-circuiting the electric field at the plate boundaries. Figures 2a and 2b show the three variants of calculated dependences of K_i^2 on H/λ for zero-order Lamb modes propagating in a YZ-cut $LiNbO_3$ plate. From these figures, one can see that the dependence of K^2 on H/λ has a complicated form with maxima at certain values of H/λ (see curves *1–3*). With an increase in the thickness of the piezoelectric plate $H > 3\lambda$, the phase velocities of both zero modes (curves *4*), approach the velocity of a SAW in a semi-infinite medium (V_{SAW} = 3.487 km/s): one from below, starting from the zero value, and the other from above, starting from a value approximately equal to the velocity of the bulk longitudinal wave. However, the value of the electromechanical coupling coefficient K^2 approaches the corresponding value for the SAW ($K^2 \approx$ 4.38%) not in all cases, which is seen from Fig. 2. If the lower surface is open, the value of K^2 for the low-velocity mode (curve *1* in Fig. 2a) approaches the corresponding value for the SAW, while K^2 for the high-velocity mode (curve *1* in Fig. 2b) approaches zero. If the lower surface is short-circuited, the quantities behave conversely (curves *2* in Figs. 2a, 2b). If we calculate K^2 by Eq. (8) from the velocities determined on the condition that both surfaces are either open or short-circuited, then, for both zero modes, as the plate thickness grows, K^2 approaches the value corresponding to the SAW (curves *3* in Figs. 2a, 2b). In addition, in this case, we have the highest value of K^2 equal to about 11% for the low-velocity mode near H/λ = 0.55 (curve *3* in Fig. 2a). The curves in Fig. 2 also show that, for any plate thickness, for both zero-order modes, the condition $K_3^2 = K_1^2 + K_2^2$ is satisfied (here, the subscripts correspond to the curve numbers in Fig. 2). Note that, for the orientation considered, symmetry condition (4) is satisfied and the zero-order Lamb modes have two components of mechanical displacement, u_1 and u_3, and an electric potential φ [11]. Figure 3 demonstrates the calculated distributions of the amplitudes of mechanical displacements u_1 and u_3 (curves u_1 and u_3) over the thickness ($H = 0.5\lambda$) of a YZ-$LiNbO_3$ plate for the high-velocity zero-order mode (here and below, the amplitudes are normalized to $u_0 = \sqrt{|u_{01}|^2 + |u_{02}|^2 + |u_{03}|^2}$,

where u_{0i} are the amplitudes at the surface $X_3 = H/2$). As is seen from Fig. 3, the distribution of the displacement amplitude u_1 over the plate thickness is symmetric and the distribution of u_3 is antisymmetric.

If the symmetry conditions (5) are satisfied, a transverse plate wave (SH wave) propagates in the piezoelectric plate. It is a shear-horizontal high-velocity wave that does not contain the component of mechanical displacement u_3 normal to the plate surface. Owing to this, the SH wave can propagate in a plate contacting a liquid without any radiation loss due to the wave energy leakage into the liquid medium. Another feature of the SH wave consists in the fact that, at a certain plate thickness, the electromechanical coupling coefficient K^2 may be very high. For example, for a lithium niobate plate, the cuts and directions were found [4, 5], in which a quasi-SH wave propagates: although, in the directions found, the symmetry conditions (5) are not satisfied and the wave has all three mechanical displacements, the condition $u_1, u_3 \ll u_2$ is satisfied. For an *XY*-cut $LiNbO_3$ plate with the thickness $H = 0.1\lambda$, the electromechanical coupling coefficient is $K^2 \approx 35\%$ and the phase velocity is $V = 4.372$ km/s.

In the present study, the parameters of SH waves in piezoelectric plates with a strong piezoelectric coupling are theoretically calculated. We considered a potassium niobate crystal ($KNbO_3$) [12] and a lead-treated potassium niobate crystal (PKN) [13] belonging to the rhombic and orthorhombic systems, respectively. In these crystals, symmetry condition (5) is satisfied for the orientations (0°, 90°, 180°*m*), where $m = 0, 1, 2, \ldots$ [14]. Figure 4 displays the calculated velocities *V* (curves *V*1, *V*2, *V*3, and *V*4), which were obtained under the condition that both surfaces were open, and the quantity K^2 (curves *k*1, *k*2, *k*3, and *k*4), calculated under the condition that the lower surface was open, versus the normalized plate thickness H/λ for the crystals (90°, 90°, 0°) $LiNbO_3$, (0°, 90°, 0°) $KNbO_3$, (0°, 90°, 0°) PKN, and (90°, 90°, 0°) $LiTaO_3$. The materials constants for $KNbO_3$, PKN, $LiNbO_3$, and $LiTaO_3$ were taken from [12, 13, 15]. As is seen from Fig. 4, the maximal values of K^2 are as follows: for *XY*-cut $LiNbO_3$, $K^2 \approx 35\%$ and the phase velocity $V \approx 4.35$ km/s at $H/\lambda = 0.06$; for *YX*-cut $KNbO_3$, $K^2 = 99.3\%$ and $V = 4.67$ km/s at $H/\lambda = 0.12$; for *YX*-cut PKN, $K^2 = 54.5\%$ and $V = 3.04$ km/s at $H/\lambda = 0.02$; and for *XY*-cut $LiTaO_3$, $K^2 = 10.7\%$ and $V = 3.75$ km/s at $H/\lambda = 0.06$. Such record high values of K^2 in these crystals open up the possibilities for an efficient control of the SH wave velocity, e.g., by bringing a conducting screen near the plate surface. This feature can be used in developing high-efficiency acoustoelectronic sensors.

We also studied theoretically the temperature properties of Lamb waves in a langasite (LGS) piezoelectric plate with the (0°, 138.5°, 23°) orientation, which is thermostable for a SAW [16]. The calculations showed

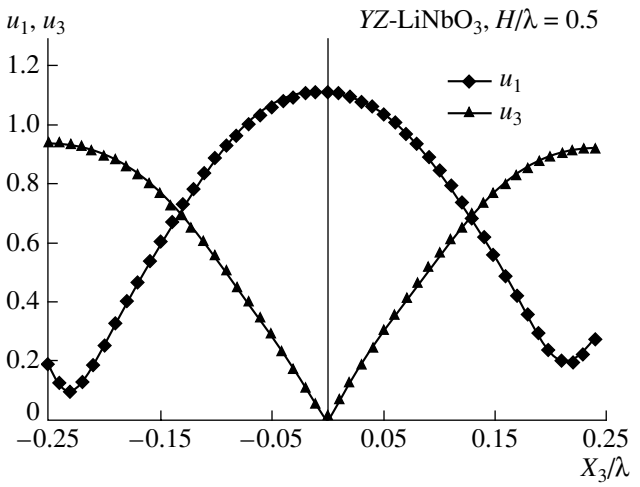

Fig. 3. Distributions of the relative amplitudes u_1 and u_3 over the thickness of a *YZ*-cut $LiNbO_3$ plate for the high-velocity zero-order mode.

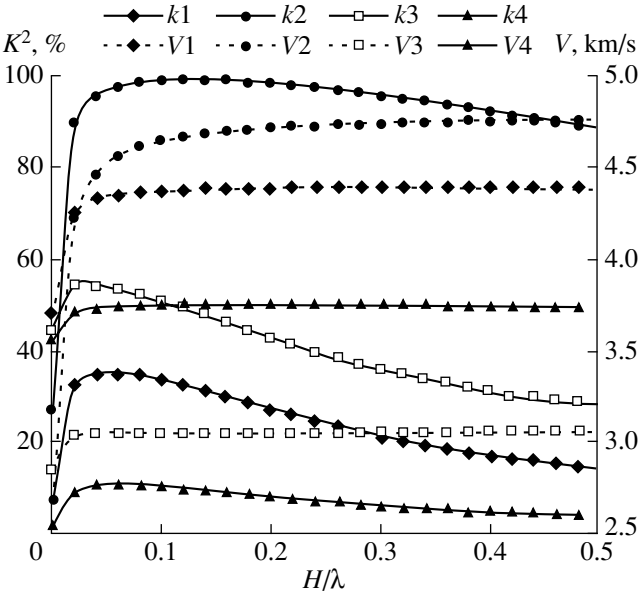

Fig. 4. Velocity of SAW propagation *V* and the electromechanical coupling coefficient K^2 versus the normalized plate thickness H/λ for (*V*1, *k*1) *XY*-cut $LiNbO_3$, (*V*2, *k*2) *YX*-cut $KNbO_3$, (*V*3, *k*3) *YX*-cut PKN, and (*V*4, *k*4) *XY*-cut $LiTaO_3$.

that the value of the temperature coefficient of delay [10] rather strongly depends on the thickness of the piezoelectric plate and on the mode number. Figure 5 shows the computed values of this coefficient for low- and high-velocity zero-order Lamb modes versus H/λ. The value of the temperature coefficient of delay is close to zero for the high-velocity mode at the plate thickness $H \approx 0.6\lambda$, $H \approx 1.3\lambda$, and $H > 1.5\lambda$ (both surfaces are open); for the low-velocity zero-order mode,

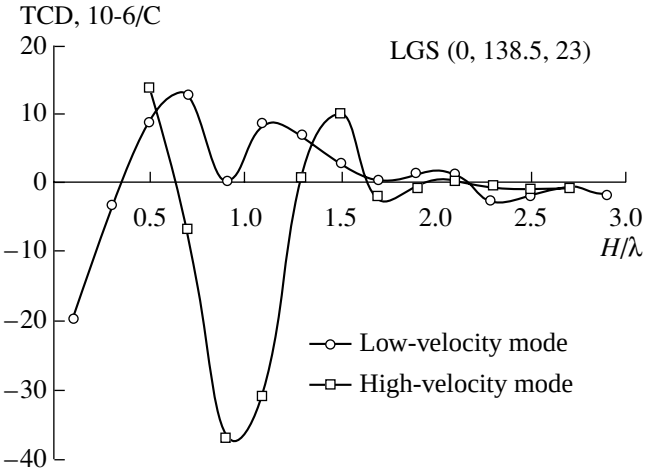

Fig. 5. Temperature coefficient of delay versus the normalized plate thickness H/λ for the low- and high-velocity zero-order Lamb modes in a (0°, 138.5°, 23°) LGS plate.

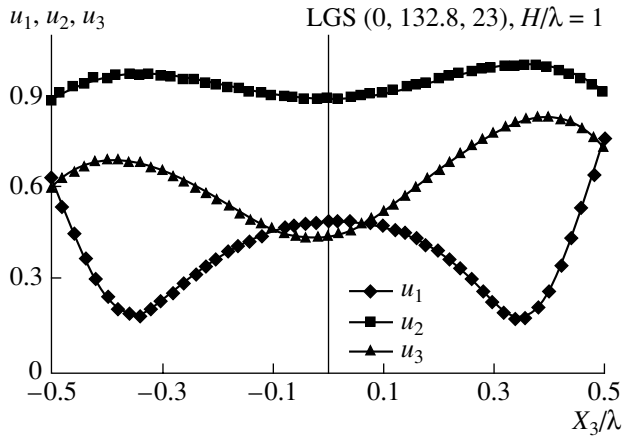

Fig. 6. Distributions of the relative amplitudes U_1, U_2, and U_3 over the thickness of a (0°, 138.5°, 23°) LGS plate. The plate thickness is $H = \lambda$.

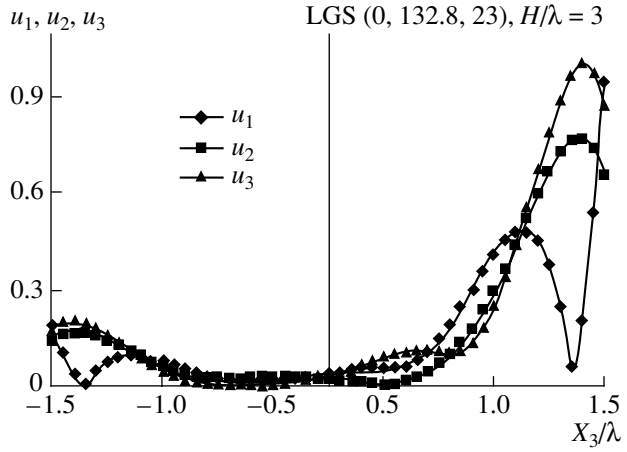

Fig. 7. Distributions of the relative amplitudes U_1, U_2, and U_3 over the thickness of a (0°, 138.5°, 23°) LGS plate. The plate thickness is $H = 3\lambda$.

it is close to zero at $H = 0.35\lambda$, $H \approx 0.9\lambda$, and $H > 1.7\lambda$. The materials constants for LGS were taken from [17].

Now, we consider the distribution of the mechanical displacements u_1, u_2, and u_3 of the Lamb modes for different ratios H/λ. Figure 6 shows the distributions of the normalized amplitudes of mechanical displacements for the low-velocity zero-order mode (velocity V = 2.686 km/s, both surfaces are open) in a (0°, 138.5°, 23°) LGS piezoelectric plate of thickness $H = \lambda$. It is seen from Fig. 6 that the distribution of the amplitudes of mechanical displacements over the plate thickness is of a complex character. There are several characteristic maxima and minima of the displacement values across the plate thickness (curves U_1, U_2, and U_3). At the thickness $H = 3\lambda$ (Fig. 7), the structure of this mode (V = 2.729 km/s) approaches the structure of a common SAW (V = 2.733 km/s). As is seen from Fig. 7, all mechanical displacements are concentrated near the plate boundaries and die out in the middle of the plate (curves U_1, U_2, and U_3).

Thus, in this paper, we calculated the main characteristics of plate waves propagating in $LiNbO_3$, $LiTaO_3$, LGS, $KNbO_3$, and PKN piezoelectric plates. The cuts and directions in which SH waves have record high values of the electromechanical coupling coefficient are determined. In particular, for the *YX*-cut $KNbO_3$ plate, the value of this coefficient is K^2 = 99.3%, and for the *YX*-cut PKN plate, K^2 = 54.5%. It is shown that, at certain plate thickness values, low- and high-velocity Lamb modes propagating in a (0°, 138.5°, 23°) LGS plate have zero values of the temperature coefficient of delay.

REFERENCES

1. E. Adler, IEEE Trans. Ultrason. Ferroelectr. Freq. Control **36**, 223 (1989).
2. Y. Jin and S. G. Joshi, in *Abstracts of IEEE Ultrasonic Symposium* (IEEE, 1993), Vol. 2, p. 847.
3. O. Borovkov and I. Kucherov, Ukr. Fiz. Zh. **17**, 1980 (1972).
4. B. D. Zaitsev, S. G. Joshi, and I. E. Kuznetsova, in *Proceedings of IEEE Ultrasonic Symposium* (1998), p. 419.
5. S. G. Joshi, B. D. Zaĭtsev, and I. E. Kuznetsova, Akust. Zh. **47**, 336 (2001) [Acoust. Phys. **47**, 282 (2001)].
6. I. V. Anisimkin, Yu. V. Gulyaev, and V. I. Anisimkin, in *Proceedings of IEEE Ultrasonic Symposium* (2001), p. 423.
7. F. Teston, G. Feuillard, and L. Tessier, IEEE Trans. Ultrason. Ferroelectr. Freq. Control **45**, 1266 (1995).
8. S. Balandras, J. Briot, and G. Martin, in *Proceedings of IEEE Ultrasonic Symposium* (1996), p. 459.

9. I. A. Viktorov, *Rayleigh and Lamb Waves: Physical Theory and Applications* (Nauka, Moscow, 1966; Plenum Press, New York, 1967).
10. *Surface Wave Filters: Design, Construction, and Use*, Ed. by H. Mathews (Wiley, New York, 1977; Radio i Svyaz', Moscow, 1981).
11. E. Adler, IEEE Trans. Ultrason. Ferroelectr. Freq. Control **36** (2), 223 (1989).
12. M. Zgonik, R. Schlesesser, and I. Biaggio, J. Appl. Phys. **74**, 1287 (1993).
13. R. Sun, S. Fan, and J. Wu, in *Proceedings of IEEE International Frequency Control Symposium* (1996), p. 113.
14. M. Yu. Dvoesherstov, S. G. Petrov, and V. I. Cherednik, Izv. Vyssh. Uchebn. Zaved., Radiofiz. **43** (5), 445 (2000).
15. G. Covacs, M. Anhorn, H. Engan, *et al.*, in *Proceedings of IEEE Ultrasonic Symposium* (1990), p. 435.
16. K. Inoue and K. Sato, Jpn. J. Appl. Phys. **37**, 2909 (1998).
17. Y. Pisarevsky, P. Senyshenkov, B. Mill, and N. Moiseeva, in *Proceedings of IEEE International Frequency Control Symposium* (1998), p. 742.

Translated by A. Svechnikov